Available online at www.sciencedirect.com
SCIENCE DIRECT®
Optics Communications 246 (2005) 45–56
OPTICS COMMUNICATIONS
www.elsevier.com/locate/optcom

Highly directed transmission of multipole radiation by an interface

Henk F. Arnoldus *, John T. Foley

Department of Physics and Astronomy, Mississippi State University, P.O. Drawer 5167, Mississippi State, MS 39762-5167, USA

Received 2 September 2004; accepted 22 October 2004

Abstract

Electromagnetic multipole radiation can have a highly directed peak in its angular intensity distribution when transmitted through an interface (xy-plane) with a medium that has a higher index of refraction. We show that the possible occurrence of such a peak depends on the order of the multipole. It is also shown that the peak intensity is determined uniquely by the intensity of the multipole radiation in the xy-plane in the absence of the interface. This peak occurs at the slightest difference in index of refraction of the two media, and when the indices of refraction are almost equal, the peak appears just below the interface in the denser medium, and it has an intensity of four times the intensity in the xy-plane of the unbounded multipole.
© 2004 Elsevier B.V. All rights reserved.

PACS: 03.50.De; 42.25.Bs; 42.25.Gy; 42.25.Hz
Keywords: Multipole radiation; Transmission; Reflection; Interface; Interference

1. Introduction

Magnetic or electric multipole radiation is a spherical wave emanating from the location of the multipole, and the radiation is characterized by its order (ℓ,m). For $\ell = 1,2,\ldots$ we have dipole, quadrupole,... radiation, and given ℓ, the possible values of m are $m = -\ell,-\ell+1,\ldots,\ell$ [1]. Multipole radiation has the typical dipole, quadrupole,... angular intensity distribution, depending on the order (ℓ,m). For a given ℓ and m, this radiation pattern is the same for magnetic and electric multipoles. Alternatively, multipole radiation can be represented by an angular spectrum, which is a superposition of plane waves of the form $\exp(i\mathbf{k}\cdot\mathbf{r})$ [2,3]. When the radiation is monochromatic with angular frequency ω, and when the multipole is embedded in a medium with index of refraction n_1 (assumed to be positive),

* Corresponding author. Tel.: +1 662 325 2919; fax: +1 662 325 8898.
E-mail addresses: arnoldus@ra.msstate.edu (H.F. Arnoldus), jtf1@ra.msstate.edu (J.T. Foley).

0030-4018/$ - see front matter © 2004 Elsevier B.V. All rights reserved.
doi:10.1016/j.optcom.2004.10.083

then the wave number is $k = n_1\omega/c$. The angular spectrum representation involves adopting a preferred direction in space, and this direction will be taken as the z-axis. The wave vector can then be written as $\mathbf{k} = \mathbf{k}_\parallel + k_z\mathbf{e}_z$, where the vector $\mathbf{k}_\parallel$ is in the xy-plane. This $\mathbf{k}_\parallel$ is the integration variable of the representation, and its range covers the entire xy-plane. For a given $\mathbf{k}_\parallel$, the z-component of the wave vector must then satisfy the relation $k_z^2 = (n_1\omega/c)^2 - k_\parallel^2$, which only leaves the sign of k_z to be determined. In $\exp(i\mathbf{k}\cdot\mathbf{r})$, the vector $\mathbf{r}$ is the field point. For $k_\parallel < n_1\omega/c$, k_z is real, and we take k_z positive (negative) for $z > 0$ ($z < 0$). The partial wave $\exp(i\mathbf{k}\cdot\mathbf{r})$ then travels away from the xy-plane at both sides. On the other hand, for $k_\parallel > n_1\omega/c$, k_z is imaginary, and we shall take k_z as positive (negative) imaginary for $z > 0$ ($z < 0$). These are the evanescent waves of the angular spectrum, and they decay away from the xy-plane at both sides, while traveling along the xy-plane with wave vector $\mathbf{k}_\parallel$.

Of particular interest is the situation where the multipole, assumed to be of atomic dimensions, is located a distance H above an interface with a medium with index of refraction n_2, as shown schematically in Fig. 1. The radiation reflects and refracts at the interface, thereby modifying the radiation pattern. The angular spectrum representation with partial waves of the form $\exp(i\mathbf{k}\cdot\mathbf{r})$, accounts for the field of a multipole located at the origin of coordinates. An advantage of the angular spectrum is that the location of the multipole can easily be shifted. When the multipole is located on the z-axis we simply replace $\exp(i\mathbf{k}\cdot\mathbf{r})$ by $\exp[i\mathbf{k}\cdot(\mathbf{r} - H\mathbf{e}_z)]$ in the representation. Effectively, the xy-plane becomes the plane $z = H$, and the partial waves now travel or decay away from the plane $z = H$. As indicated in Fig. 1, the waves in $z > H$ travel away from the interface and to the far field where they can be observed with a detector. We shall call these the directly emitted (de) waves. Clearly, only the traveling waves of the angular spectrum will contribute to the radiation pattern, since the evanescent waves in $z > H$ die out in the z-direction on a length scale of about a wavelength. The partial waves in $0 < z < H$ serve as the incident (inc) waves, giving rise to the reflected (r) and transmitted (t) waves at the interface. In $z > H$, both the de- and the r-waves travel towards the detector, giving rise to interference.

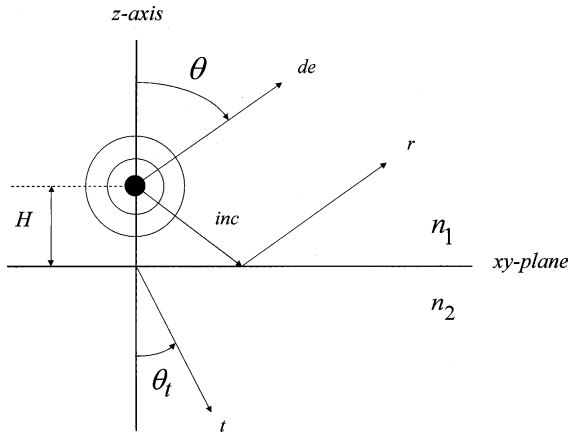

Fig. 1. Schematic illustration of a multipole located a distance H above an interface between media with indices of refraction n_1 and n_2. The circles represent the spherical multipole wave. In an angular spectrum representation this radiation field is resolved in plane waves that travel directly towards the detector (de) and waves that are incident on the surface (inc). An incident wave is reflected (r) and transmitted (t), as indicated by the corresponding arrows. The angle of observation in $z > H$ is the polar angle θ with the positive z-axis, and in $z < 0$ the observation direction is expressed in the transmission angle θ_t with the negative z-axis.

Each incident wave from the angular spectrum of the multipole gives also rise to a transmitted wave in the medium with index of refraction n_2 (assumed positive). If we indicate by θ_i the angle of incidence and by θ_t the angle of transmission, then Snell's law gives $n_1\sin\theta_i = n_2\sin\theta_t$ provided that this equation has a solution θ_t. If $n_2 < n_1$, there exists a critical angle of incidence θ_c for which the angle of transmission becomes $\theta_t = \pi/2$:

$$\sin\theta_c = \frac{n_2}{n_1}. \tag{1}$$

When the angle of incidence exceeds the critical angle, the transmitted wave is an evanescent wave, which will not contribute to the far-field intensity in $z < 0$. On the other hand, for $n_2 > n_1$ there exists an angle of transmission θ_t for which the corresponding angle of incidence approaches $\pi/2$. We call this the anti-critical angle θ_{ac}, which is given by [4]

$$\sin\theta_{ac} = \frac{n_1}{n_2}. \tag{2}$$

Any incident traveling wave with $0 \leqslant \theta_i < \pi/2$ is transmitted in the cone $0 \leqslant \theta_t < \theta_{ac}$. However, the angular spectrum of the radiation emitted by the multipole also contains evanescent waves which can be converted into traveling waves at the interface. The equivalent of Snell's law becomes that both the incident and the transmitted wave have the same $\mathbf{k}_\parallel$. Any radiation detected in the far field outside the cone $0 \leqslant \theta_t < \theta_{ac}$ has its origin in evanescent waves from the source. Since these waves emanate from the plane $z = H$ and decay in the direction towards the surface, they will only yield a substantial contribution to the field in $\theta_{ac} < \theta_t < \pi/2$ if the distance H between the multipole and the surface is about a wavelength or less.

It has long been recognized that for the problem of reflection and refraction of radiation by a plane interface from a localized source the angular spectrum representation is superbly suited since the reflection and transmission of each partial wave is simply accounted for by the appropriate Fresnel coefficients for reflection and transmission of a plane wave [5]. This method has been applied to obtain the radiation pattern of an electric dipole near an interface [6–8], although other approaches have yielded similar results [9,10]. The predictions have been confirmed experimentally [11,12], including the existence of the anti-critical angle. The applicability of the method, however, hinges on the availability of an angular spectrum representation of the source field, since this field is the incident field on the interface. An angular spectrum representation of the multipole fields was derived by Devaney and Wolf [13,14], based on a theorem due to Erdélyi [15]. Recently, we have obtained an alternative angular spectrum representation [16], which is more appropriate for the reflection and transmission problem, and with this result we have evaluated the radiation pattern of a multipole near an interface [17]. In this communication, we show that the transmitted multipole field can be highly directed along the anti-critical angle, and we derive a criterion for the occurrence of this effect.

2. Intensity distribution

We consider the situation of Fig. 1 with the multipole located a distance H above the interface and embedded in a medium with index of refraction n_1. The power per unit solid angle will be normalized as

$$\frac{dP}{d\Omega} = P_1 \mathcal{N}_{\ell m}(\hat{\mathbf{r}};\alpha), \tag{3}$$

with P_1 the power emitted by the multipole in medium n_1, but without any boundaries, and $\alpha = \mathrm{m}$ and $\alpha = \mathrm{e}$ for a magnetic and an electric multipole, respectively. The normalized intensity distribution $\mathcal{N}_{\ell m}(\hat{\mathbf{r}};\alpha)$ depends on the direction of observation $\hat{\mathbf{r}}$, but due to symmetry it only depends on the polar angle θ in $z > H$ or the angle of transmission θ_t in $z < 0$. It is also independent of the sign of m, so we shall consider $m \geqslant 0$ only.

The intensity distribution in $z > H$ for a magnetic multipole is given by [17]

$$\mathcal{N}_{\ell m}(\hat{\mathbf{r}};\mathrm{m}) = |1 + (-1)^{\ell+m} R_p e^{2in_1 h\cos\theta}|^2 f_{\ell m}(\cos\theta) + |1 - (-1)^{\ell+m} R_s e^{2in_1 h\cos\theta}|^2 g_{\ell m}(\cos\theta). \tag{4}$$

Here, R_p and R_s are the Fresnel reflection coefficients for p- and s-polarized plane waves, respectively, and $h = H\omega/c$ is the dimensionless distance between the multipole and the interface. The terms "1" inside the absolute value signs represent the de-waves, and the factors $\exp(2in_1 h\cos\theta)$ multiplying the Fresnel coefficients account for the difference in travel distance (retardation) of the r-waves with respect to the de-waves. The intensity distribution for an electric multipole is also given by Eq. (4), but the Fresnel coefficients R_p and R_s have to be exchanged. The functions $f_{\ell m}(\zeta)$ and $g_{\ell m}(\zeta)$ are defined in Appendix A. Without the interface we have $R_p = R_s = 0$ and Eq. (4) becomes

$$\mathcal{N}_{\ell m}(\hat{\mathbf{r}};\alpha) = f_{\ell m}(\cos\theta) + g_{\ell m}(\cos\theta), \tag{5}$$

both for $\alpha = \mathrm{m}$ and $\alpha = \mathrm{e}$, and therefore $f_{\ell m}(\cos\theta) + g_{\ell m}(\cos\theta)$ represents the intensity distribution of an (ℓ,m) multipole in unbounded space (also for $z < 0$, see below). This far-field distribution is independent of the height H. The appearance of two functions $f_{\ell m}$ and $g_{\ell m}$ comes from

the splitting into p- and s-polarized waves. These functions are independent of the index of refraction n_1 and are the same for magnetic and electric multipoles of the same order (ℓ,m). The Fresnel coefficients are explicitly

$$R_{\rm p} = \frac{\cos\theta - r\sqrt{1-r^2\sin^2\theta}}{\cos\theta + r\sqrt{1-r^2\sin^2\theta}}, \tag{6}$$

$$R_{\rm s} = \frac{r\cos\theta - \sqrt{1-r^2\sin^2\theta}}{r\cos\theta + \sqrt{1-r^2\sin^2\theta}}, \tag{7}$$

in terms of the parameter

$$r = \frac{n_1}{n_2}. \tag{8}$$

The intensity distribution in $z < 0$ for a magnetic multipole is

$$\mathcal{N}_{\ell m}(\hat{\mathbf{r}};\mathrm{m}) = \frac{1}{r}\mathrm{e}^{2n_1 h \mathrm{Im} w}[|\hat{T}_{\rm p}|^2 f_{\ell m}(w) + |\hat{T}_{\rm s}|^2 g_{\ell m}(w)], \tag{9}$$

and for an electric multipole we exchange the Fresnel transmission coefficients $\hat{T}_{\rm p}$ and $\hat{T}_{\rm s}$. The parameter w appearing as the arguments of the functions $f_{\ell m}$ and $g_{\ell m}$ is defined as

$$w = -\frac{1}{r}\sqrt{r^2 - \sin^2\theta_{\rm t}}, \tag{10}$$

with the understanding that the square root is taken as positive imaginary if $\sin\theta_{\rm t} > r$. In view of Eq. (2), this happens when $\theta_{\rm t} > \theta_{\rm ac}$, and this is only possible in the situation where n_2 is larger than n_1. Therefore, an imaginary w corresponds to an evanescent incident wave, given the traveling wave at angle $\theta_{\rm t}$. From Snell's law, $n_1\sin\theta_{\rm i} = n_2\sin\theta_t$, we see that $w = -\cos\theta_{\rm i}$ if the incident wave is traveling. If the incident wave is evanescent then there is no angle associated with the parameter w.

The overall factor $\exp(2n_1 h \mathrm{Im} w)$ is equal to unity if w is real, corresponding to a traveling incident wave. In this case, the angle of transmission is in the range $0 \leqslant \theta_{\rm t} < \theta_{\rm ac}$ if $n_2 > n_1$ or $0 \leqslant \theta_{\rm t} < \pi/2$ if $n_2 < n_1$, and there is no dependence on H in the radiation pattern. On the other hand, for an evanescent wave $\mathrm{Im}\, w$ is negative, and this exponential factor decreases rapidly with the dimensionless distance h between the multipole and the surface. This occurs for $\theta_{\rm t} > \theta_{\rm ac}$ $(n_2 > n_1)$, indicating that no radiation will be transmitted into the region $\theta_{\rm ac} < \theta_{\rm t} < \pi/2$ if H is sufficiently large.

The Fresnel coefficients $\hat{T}_{\rm p}$ and $\hat{T}_{\rm s}$ for a plane wave are modified transmission coefficients (indicated by the caret) to include the change in solid angle upon transmission, and they are explicitly

$$\hat{T}_{\rm p} = \frac{2\cos\theta_{\rm t}}{r\cos\theta_{\rm t} - w}, \tag{11}$$

$$\hat{T}_{\rm s} = \frac{2\cos\theta_{\rm t}}{\cos\theta_{\rm t} - rw}. \tag{12}$$

For $n_2 = n_1$ we have $r = 1$. Then $w = -\cos\theta_{\rm t}$ and this is $w = \cos\theta$ since $\theta > \pi/2$. We then also have $\hat{T}_{\rm p} = \hat{T}_{\rm s} = 1$, and Eq. (9) reduces to Eq. (5).

3. Onset of the radiation pattern near the interface

The far-field intensity distribution of a multipole in an unbounded medium ($r = 1$) is given by Eq. (5), and the functions $f_{\ell m}$ and $g_{\ell m}$ can be obtained from the expressions given in Appendix A. To be specific, for a dipole they are

$$f_{11}(\zeta) = \frac{3}{16\pi}, \quad g_{11}(\zeta) = \frac{3}{16\pi}|\zeta|^2, \tag{13}$$

$$f_{10}(\zeta) = 0, \quad g_{10}(\zeta) = \frac{3}{8\pi}|1-\zeta^2|, \tag{14}$$

and for a quadrupole we have

$$f_{22}(\zeta) = \frac{5}{16\pi}|1-\zeta^2|, \quad g_{22}(\zeta) = \frac{5}{16\pi}|1-\zeta^2||\zeta|^2, \tag{15}$$

$$f_{21}(\zeta) = \frac{5}{16\pi}|\zeta|^2, \quad g_{21}(\zeta) = \frac{5}{16\pi}|2\zeta^2-1|^2, \tag{16}$$

$$f_{20}(\zeta) = 0, \quad g_{20}(\zeta) = \frac{15}{8\pi}|1-\zeta^2||\zeta|^2. \tag{17}$$

In particular, for a field point in the xy-plane we have $\cos\theta = 0$, and the intensity is

$$\mathcal{N}_{\ell m}(\hat{\mathbf{r}};\alpha) = f_{\ell m}(0) + g_{\ell m}(0). \tag{18}$$

Let us first consider the transmitted field. If we set $\theta_{\rm t} = \pi/2$ in Eqs. (11) and (12) we find $\hat{T}_{\rm p} = \hat{T}_{\rm s} = 0$ for all $r \neq 1$, and therefore

$$\mathcal{N}_{\ell m}(\hat{\mathbf{r}};\alpha) = 0, \tag{19}$$

in the xy-plane. This shows that for all $r \neq 1$ the intensity in the xy-plane vanishes, whereas for $r = 1$ it is given by the right-hand side of Eq. (18). Apparently, the intensity jumps from some value (possibly zero) to zero at the slightest deviation of r from unity.

Most interesting is the case $n_2 > n_1$, so that $0 < r < 1$. Then there exists an anti-critical transmission angle θ_{ac}, given by Eq. (2), and we have $\sin\theta_{ac} = r$. At $\theta_t = \theta_{ac}$ we find $w = 0$ from Eq. (10), and this yields for the transmission coefficients

$$\hat{T}_p = \frac{2}{r}, \quad \hat{T}_s = 2. \tag{20}$$

From Eq. (9) we then obtain

$$\mathcal{N}_{\ell m}(\hat{\mathbf{r}};\mathrm{m}) = \frac{4}{r^3}\left[f_{\ell m}(0) + r^2 g_{\ell m}(0)\right] \quad (\theta_t = \theta_{ac}) \tag{21}$$

and for an electric multipole we switch $f_{\ell m}(0)$ and $g_{\ell m}(0)$.

If we now consider $r \lesssim 1$, we have $\sin\theta_{ac} \lesssim 1$ and therefore $\theta_{ac} \lesssim \pi/2$. From Eq. (21) we then find

$$\mathcal{N}_{\ell m}(\hat{\mathbf{r}};\alpha) \approx 4[f_{\ell m}(0) + g_{\ell m}(0)], \tag{22}$$

for the intensity at angle $\theta_t = \theta_{ac}$ just below the xy-plane. This result also holds for an electric multipole since exchanging $f_{\ell m}(0)$ and $g_{\ell m}(0)$ in Eq. (22) has no effect. On the other hand, for $r = 1$ the intensity in the xy-plane is given by Eq. (18), and we see that there is a difference of a factor of four. The conclusion is that for $r = 1$, the intensity in the xy-plane has some given value, given by the right-hand side of Eq. (18). Then for the slightest decrease in r, the intensity in the xy-plane drops to zero, and the value of the intensity just below the xy-plane increases by a factor of four. This holds for any multipole, and is independent of the details of the functions $f_{\ell m}$ and $g_{\ell m}$. Fig. 2 shows the appearance of this peak just below the xy-plane for the case of an electric quadrupole with $m = 1$. For increasing r, such a peak does not appear.

The radiation pattern in $z > H$ is given by Eq. (4). For a field point in (near) the xy-plane we have

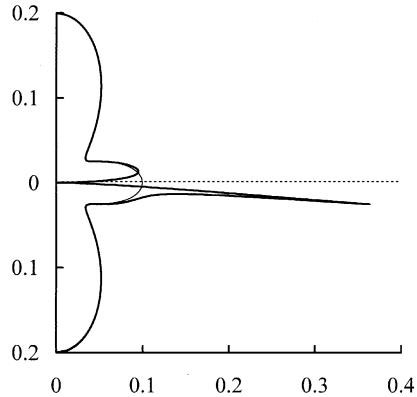

Fig. 2. Polar diagram of the radiation pattern of an electric quadrupole with $m = 1$. The vertical axis is the z-axis and the dotted line is the xy-plane. The intensity distribution is rotationally symmetric around the z-axis. The thin line is the radiation pattern for the quadrupole in unbounded space, and the thick line is for $n_1 = 1$ and $n_2 = 1.0025$. The value of r is 0.9975 and the anti-critical angle is 86°. The diagram illustrates that for $r \lesssim 1$, the intensity in the xy-plane vanishes, and that a peak appears just below the xy-plane. The peak value equals four times the value of the intensity in the xy-plane for the multipole in an unbounded medium. The parameter h was taken as 2π, but the observed effect here is independent of h.

$\theta = \pi/2$, and from Eqs. (6) and (7) we find $R_p = R_s = -1$ for all $r \neq 1$. Eq. (4) reduces to

$$\mathcal{N}_{\ell m}(\hat{\mathbf{r}};\mathrm{m}) = \begin{cases} 4f_{\ell m}(0), & \ell + m \text{ odd}, \\ 4g_{\ell m}(0), & \ell + m \text{ even}. \end{cases} \tag{23}$$

The same holds for an electric multipole, since exchanging R_p and R_s has no effect (both equal to -1). It is shown in Appendix A that the functions $f_{\ell m}$ and $g_{\ell m}$ have the property

$$f_{\ell m}(0) = 0, \quad \ell + m \text{ odd}, \tag{24}$$

$$g_{\ell m}(0) = 0, \quad \ell + m \text{ even}, \tag{25}$$

and therefore we find $\mathcal{N}_{\ell m}(\hat{\mathbf{r}};\alpha) = 0$. So, just like for the transmitted field, the intensity in the xy-plane drops from the value given by the right-hand side of Eq. (18) to zero.

For the field in $z > H$ we consider first the case $n_2 < n_1$, for which $r > 1$. Then there exists a critical angle of incidence θ_c, given by Eq. (1), which can be expressed as $\sin\theta_c = 1/r$. When we set the angle of observation θ equal to θ_c (angle of incidence equals the angle of reflection), then $1 - r^2\sin^2\theta = 0$

and the Fresnel reflection coefficients are found to be $R_p = R_s = 1$ from Eqs. (6) and (7). If we subsequently let $\theta \to \pi/2$, and thereby $r \to 1$, since $\sin\theta = \sin\theta_c = 1/r$, Eq. (4) becomes

$$\mathcal{N}_{\ell m}(\hat{\mathbf{r}};\alpha) \approx \begin{cases} 4f_{\ell m}(0), & \ell + m \text{ even}, \\ 4g_{\ell m}(0), & \ell + m \text{ odd}. \end{cases} \tag{26}$$

The result also holds for $\alpha = \mathrm{e}$, since exchanging R_p and R_s has no effect in this limit. With Eqs. (24) and (25) this can also be written as

$$\mathcal{N}_{\ell m}(\hat{\mathbf{r}};\alpha) \approx 4[f_{\ell m}(0) + g_{\ell m}(0)], \tag{27}$$

since the added term is zero. This value for $\mathcal{N}_{\ell m}(\hat{\mathbf{r}};\alpha)$ just above the xy-plane is four times the value for the unbounded multipole in the xy-plane. Fig. 3 shows this effect for an $m = 1$ quadrupole. Interesting to notice is that this behavior holds for any multipole, and is independent of the distance H between the surface and the multipole. The figure also shows that in this case of $n_2 < n_1$ there is no peak in $z < 0$, and Fig. 2 shows that for $n_2 > n_1$ there is no peak in $z > H$.

4. Highly directed transmission

For $n_2 \gtrsim n_1$ a sharp peak appears just below the xy-plane, as shown in Fig. 2. We now consider what happens to this peak when the value of n_2 increases. The intensity distribution for $z < 0$ is given by Eq. (9). The dependence on the transmission angle θ_t comes in through the overall exponential, the Fresnel coefficients and the functions $f_{\ell m}(w)$ and $g_{\ell m}(w)$, with the argument w given by Eq. (10). The functions $f_{\ell m}$ and $g_{\ell m}$ are smooth functions of their arguments, as can be seen from Eqs. (13)–(17) for dipoles and quadrupoles. The effect of the exponential is that the intensity in the region $\theta_{ac} < \theta_t < \pi/2$ will become negligible if the distance between the multipole and the interface is about a wavelength or more. The Fresnel transmission coefficients enter as $|\hat{T}_p|^2$ and $|\hat{T}_s|^2$, and it follows from Eqs. (11) and (12) that $|\hat{T}_p|^2$ and $|\hat{T}_s|^2$ have a maximum at $w = 0$, which is at $\theta_t = \theta_{ac}$. From Eq. (20) we see that the peak values are $|\hat{T}_p|^2 = 4/r^2$ and $|\hat{T}_s|^2 = 4$. Figs. 4 and 5 show $|\hat{T}_p|^2$ and $|\hat{T}_s|^2$, respectively, as a function of θ_t and for three values of r. For $n_1 = 1$ and $n_2 = 2.92$ the value of r is 0.342, and this given a peak of $|\hat{T}_p|^2 = 34$, as shown in Fig. 4. Evidently, $|\hat{T}_p|^2$ has a strong peak at $\theta_t = \theta_{ac}$, and this leads to a strong peak at the anti-critical angle in the intensity distribution. Fig. 6 illustrates the strong peak at $\theta_t = \theta_{ac}$ for an electric quadrupole with $m = 1$, and for $n_1 = 1$ and $n_2 = 1.22$ ($r = 0.82$). Already for this very moderate value of n_2 there is a highly directed transmission near the anti-critical

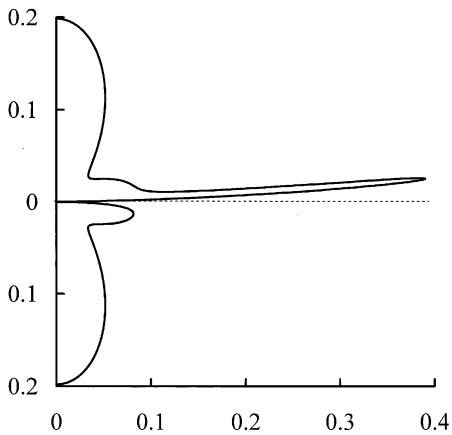

Fig. 3. Polar diagram of the radiation pattern for an $m = 1$ quadrupole for the same parameters as in Fig. 2, but with the indices of refraction n_1 and n_2 exchanged. The peak now appears above the xy-plane, and again with four times the value of the intensity in the xy-plane for an unbounded medium. The critical angle is 86° and $r = 1.0025$.

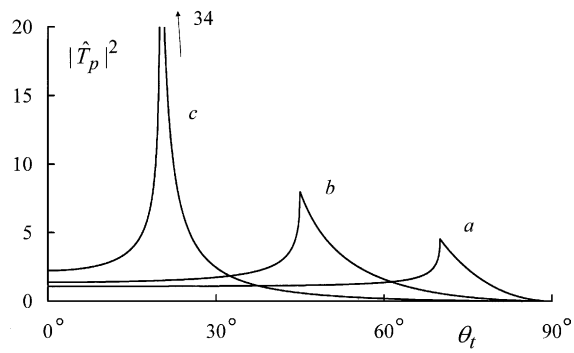

Fig. 4. Graphs of $|\hat{T}_p|^2$ versus the angle of transmission θ_t. Curves (a), (b) and (c) correspond to $r = 0.940$, 0.707 and 0.342, respectively. The peaks appear at the anti-critical angles, which are, respectively, 70°, 45°, and 20°. The heights of the peaks are given by $|\hat{T}_p|^2 = 4/r^2$, and as indicated the height for $\theta_{ac} = 20°$ is 34.

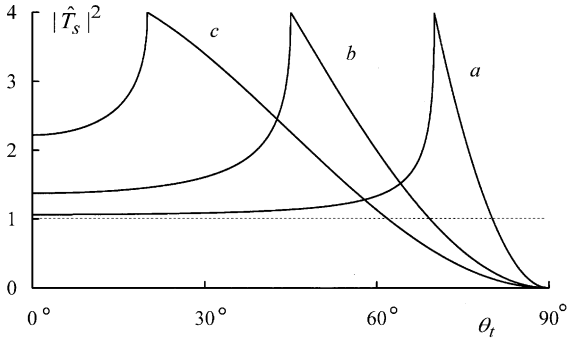

Fig. 5. Graphs of $|\hat{T}_s|^2$ versus the angle of transmission θ_t for the same parameters as in Fig. 4. The peaks here also appear at the anti-critical angles, but the peak height is $|\hat{T}_s|^2 = 4$ for all r.

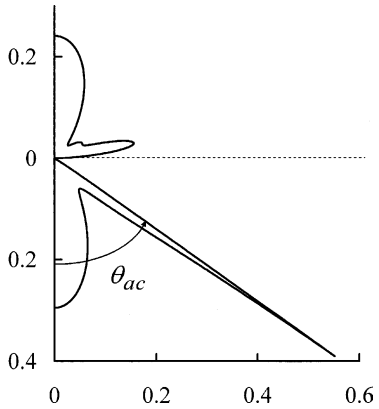

Fig. 6. Polar diagram of the intensity distribution for an electric quadrupole with $m = 1$ The parameters are the same as in Fig. 2, except that $n_2 = 1.22$. The value of r is 0.82 and the anti-critical angle is $\theta_{ac} = 55°$. The figure illustrates the emerging of the highly directed peak at θ_{ac} with decreasing value of r.

angle. In Fig. 7 we have $n_2 = 2.45$ ($r = 0.408$), with all other parameters the same as in Fig. 6. The peak height at $\theta_t = \theta_{ac}$ is given by Eq. (21) with $f_{\ell m}$ and $g_{\ell m}$ exchanged. From Eq. (16) we have for the $m = 1$ quadrupole $f_{21}(0) = 0$, $g_{21}(0) = 5/(16\pi)$, which gives a peak height of $5/(4\pi r^3) = 5.8$.

5. Conditions for highly directed transmission

For an unbounded medium, the value of the intensity in the xy-plane is given by Eq. (18), and for $0 < r < 1$ the value of the intensity at the anti-

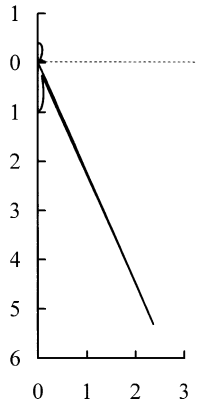

Fig. 7. Same as Fig. 6, but with $n_2 = 2.45$. Here, $r = 0.408$ and $\theta_{ac} = 24°$. The peak value of the intensity at θ_{ac} is 5.8.

critical angle is given by Eq. (21). We notice that the arguments of the functions $f_{\ell m}(\zeta)$ and $g_{\ell m}(\zeta)$ are $\zeta = 0$ in both expressions. The highly directed peak is a result of the overall factor $1/r^3$ in Eq. (21), which comes from the value of $|\hat{T}_p|^2$ at $\theta_t = \theta_{ac}$ and the factor $1/r$ in Eq. (9). However, from Eq. (24) we see that $f_{\ell m}(0) = 0$ for $\ell + m$ odd. In that case, Eq. (21) reduces to $\mathcal{N}_{\ell m}(\hat{\mathbf{r}}; \mathrm{m}) = 4g_{\ell m}(0)/r$, and the term responsible for the highly directed peak has disappeared. In other words, the strong peak in $|\hat{T}_p|^2$ is multiplied by a factor which is identically zero. The remaining term comes from $|\hat{T}_s|^2$, which still has a peak at $\theta_t = \theta_{ac}$, but the peak is much weaker.

Let us consider $\ell + m$ even, so that $g_{\ell m}(0) = 0$. For both a magnetic and an electric multipole in an unbounded medium we have in the xy-plane

$$\mathcal{N}_{\ell m}(\hat{\mathbf{r}}; \alpha) = f_{\ell m}(0). \tag{28}$$

For $0 < r < 1$ the values at the anti-critical angle are

$$\mathcal{N}_{\ell m}(\hat{\mathbf{r}}; \mathrm{m}) = \frac{4}{r^3} f_{\ell m}(0), \tag{29}$$

$$\mathcal{N}_{\ell m}(\hat{\mathbf{r}}; \mathrm{e}) = \frac{4}{r} f_{\ell m}(0). \tag{30}$$

For $r \to 1$ we have $\theta_{ac} \to \pi/2$, and both expressions approach $\mathcal{N}_{\ell m}(\hat{\mathbf{r}}; \alpha) \approx 4f_{\ell m}(0)$. For decreasing r, θ_{ac} decreases since $\sin\theta_{ac} = r$, and the values at the peak for the magnetic and electric multipole start to differ. From Eq. (29) we see that the peak value for a magnetic multipole is $4/r^3$ times the

value in the xy-plane for the unbounded multipole, and this gives rise to the highly directed peak at $\theta_t = \theta_{ac}$. The peak value for the electric multipole is $4/r$ times the value in the xy-plane for the unbounded multipole, and this corresponds to a weak peak. This also shows that the peak value, both for a strong and a weak peak, is uniquely determined by the value $f_{\ell m}(0)$ of the intensity in the xy-plane for an unbounded multipole. Then, it is shown in Appendix A that

$$f_{\ell 0}(0) = 0. \tag{31}$$

This implies that for $m = 0$ both the weak and the strong peak vanish, and we have $\mathcal{N}_{\ell m}(\hat{\mathbf{r}};\alpha) = 0$ at $\theta_t = \theta_{ac}$. This can be seen as a result of the fact that for $m = 0$ the intensity in the xy-plane for the unbounded multipole also vanishes, so when multiplied by $4/r^3$ for the strong peak or by $4/r$ for the weak peak, it remains zero. So, for $\ell + m$ even, the magnetic multipole has a strong peak and the electric multipole has a weak peak, unless $m = 0$ (and therefore ℓ even), in which case $\mathcal{N}_{\ell m}(\hat{\mathbf{r}};\alpha) = 0$ at $\theta_t = \theta_{ac}$. It is shown in Appendix A that no other "accidental" zeros of $f_{\ell m}(0)$ occur, other than the one given by Eq. (31). For $\ell + m$ odd we have $f_{\ell m}(0) = 0$, and the same considerations hold with the roles of the magnetic and electric multipoles exchanged. An "accidental" zero as in Eq. (31) does not occur for $g_{\ell m}(0)$, as proved in Appendix A. Therefore, for $\ell + m$ odd the electric multipole has a strong peak and the magnetic multipole has a weak peak. We summarize these considerations as follows: For $n_2 > n_1$ there is a highly directed transmission peak at $\theta_t = \theta_{ac}$ if $\ell + m$ even, but $m \neq 0$, for a magnetic multipole and for $\ell + m$ odd for an electric multipole. If there is no highly directed peak, then there is a weak peak, unless ℓ even and $m = 0$, in which case the intensities of both the magnetic and electric multipoles are zero at the anti-critical angle.

For a dipole we have $\ell = 1$, and therefore an $m = 1$ magnetic dipole and an $m = 0$ electric dipole have a highly directed peak, whereas the $m = 0$ magnetic dipole and the $m = 1$ electric dipole have a weak peak. For a dipole it is not possible to have $\mathcal{N}_{1m}(\hat{\mathbf{r}};\alpha) = 0$ at $\theta_t = \theta_{ac}$.

For an electric quadrupole ($\ell = 2$), we have a highly directed peak for $m = 1$, as is illustrated in Fig. 7. For $m = 2$ we then expect a weak peak, and this is shown in Fig. 8. The radiation is still mainly directed along the anti-critical angle, but the intensity is more than a factor of five lower than for the case $m = 1$. For $m = 0$, we have $\mathcal{N}_{20}(\hat{\mathbf{r}};\mathrm{e}) = 0$ at $\theta_t = \theta_{ac}$, since ℓ is even, and this is illustrated in Fig. 9. For a magnetic quadrupole we have a highly directed peak for $m = 2$, a weak peak for $m = 1$ and $\mathcal{N}_{20}(\hat{\mathbf{r}};\mathrm{m}) = 0$ at $\theta_t = \theta_{ac}$.

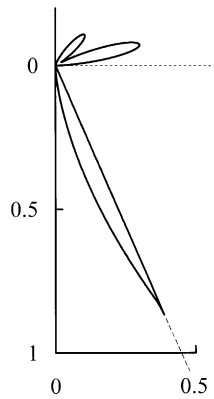

Fig. 8. Polar diagram of the intensity distribution of an electric quadrupole for the same parameters as in Fig. 7, but with $m = 2$. In this case there is no highly directed peak at θ_{ac} (indicated by the dashed line), but a weak peak.

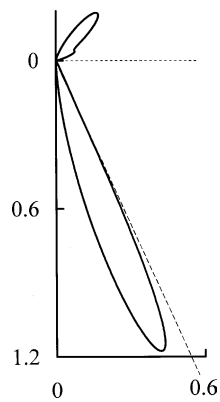

Fig. 9. Polar diagram of the intensity distribution of an electric quadrupole for the same parameters as in Fig. 7, but with $m = 0$. For this case of $\ell = 2$, $m = 0$, the intensity at the anti-critical angle vanishes. The selection rule predicts no strong peak, but also the weak peak disappears because of $f_{20}(0) = 0$.

In order to put the value of the highly directed peak to scale we consider an observation point on the negative z-axis, e.g., $\theta_t = 0$. From Eq. (10) we have $w = -1$, and from Eqs. (11) and (12) we obtain

$$\hat{T}_p = \hat{T}_s = \frac{2}{1+r}. \tag{32}$$

The intensity on the z-axis then becomes with Eq. (9)

$$\mathcal{N}_{\ell m}(\hat{\mathbf{r}};\alpha) = \frac{4}{r(1+r)^2}[f_{\ell m}(-1) + g_{\ell m}(-1)], \tag{33}$$

both for a magnetic and an electric multipole, and independent of the distance H. For $r = 1$ this is $\mathcal{N}_{\ell m}(\hat{\mathbf{r}};\alpha) = f_{\ell m}(-1) + g_{\ell m}(-1)$. Therefore, the intensity at $\theta_t = 0$ in the presence of the interface equals $4/[r(1 + r^2)]$ times the value for the intensity without the interface. On the other hand, the value of the highly directed peak is $4/r^3$ times the value of the intensity in the xy-plane for the multipole in an unbounded medium, and for the weak peak this multiplication factor was $4/r$. For r sufficiently small we have $4/[r(1 + r^2)] \approx 4/r$, showing that the value on the z-axis grows at about the same rate with decreasing r as the weak peak. The highly directed peak is a factor of $1/r^2$ larger than a corresponding weak peak and, in order of magnitude, than the value of the intensity at $\theta_t = 0$. For the case of Fig. 7 we have $1/r^2 = 6$, which expresses that the highly directed peak is about six times as strong as the transmitted intensity at other angles.

In the examples above, the dimensionless distance h between the multipole and the interface was taken as $h = 2\pi$, corresponding to one wavelength. For this distance, the evanescent waves emanating from the multipole do not reach the surface with sufficient amplitude to contribute to the intensity in $z < 0$. Evanescent waves that do reach the surface can be converted into traveling waves, provided they have the correct value of $k_\parallel$, and these traveling waves are observable in the region $\theta_{ac} < \theta_t < \pi/2$. For Fig. 10 we have set $h = 0$, and we see the appearance of a large lobe for $\theta_t > \theta_{ac}$. This lobe is entirely due to evanescent multipole waves, and we conclude that if the distance h is very small, the highly directed peak, although still present, is obscured by the dominating intensity that has its origin in evanescent waves. It was shown in [18] that for electric dipole radiation under certain circumstances almost all transmitted power could be attributed to evanescent waves.

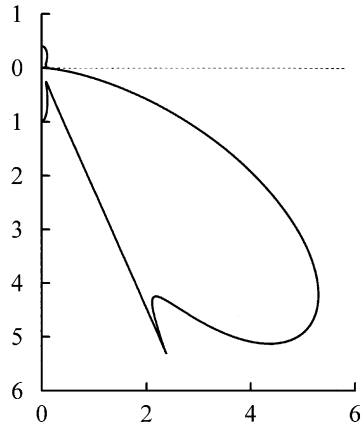

Fig. 10. Intensity distribution for an electric quadrupole for the same parameters as in Fig. 7, but with $h = 0$. The large lobe that appears at $\theta_t > \theta_{ac}$ comes from evanescent multipole waves which are converted into traveling waves at the interface.

6. Intensity distribution in $z > H$

For $n_1 \gtrsim n_2$ a highly directed peak appears just above the xy-plane with a peak intensity of four times the value in the xy-plane for an unbounded multipole, as shown in Fig. 3. This onset of the radiation pattern is the same as for the transmitted waves in the case $n_2 \lesssim n_1$. For the transmitted waves, the strong peak came from the fact that the Fresnel transmission coefficient for p-waves grows as $2/r$ at the anti-critical angle. For the reflected field, however, we have $R_p = R_s = 1$ at θ_c for all $r > 1$, and hence there is no growing of the peak value in the intensity at $\theta = \theta_c$. For $\theta < \theta_c$ we see from Eqs. (6) and (7) that $|R_\sigma| < 1$, $\sigma = $ s,p, and for $\theta > \theta_c$ the square root is positive imaginary so that $|R_\sigma| = 1$. For the factors multiplying the functions $f_{\ell m}(\cos\theta)$ and $g_{\ell m}(\cos\theta)$ in Eq. (4) we then have

$$|1 \pm (-1)^{\ell+m} R_\sigma e^{2in_1 h\cos\theta}|^2 \leqslant 4, \tag{34}$$

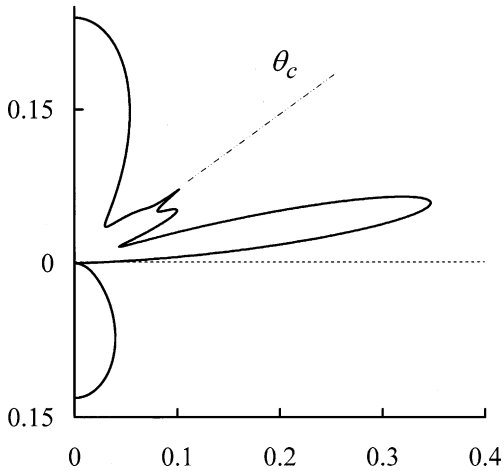

Fig. 11. Radiation pattern of an electric quadrupole with $m = 1$. The parameters are $h = 2\pi$, $n_1 = 1.22$, $n_2 = 1$, for which the critical angle is $\theta_c = 55°$. The figure illustrates that there is a peak at the critical angle, but that the main peak, the lobe at the large angle, comes from interference between reflected and directly emitted waves.

and therefore the intensity in $z > H$ is at most four times the value of the intensity for an unbounded multipole at the same angle θ.

Another difference with the transmitted field is that for $z > H$ we have interference between the reflected waves and the directly emitted waves. Fig. 11 shows that there still is a peak in the intensity distribution at the critical angle, but the large lobe at the larger angle is a result of interference, and this dominates the radiation pattern. Fig. 12 illustrates that for a smaller θ_c there is no peak anymore at θ_c, and the main feature of the intensity distribution is the interference structure.

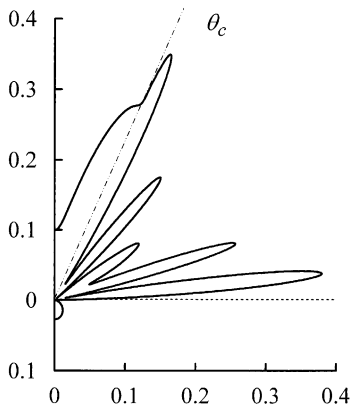

Fig. 12. Intensity distribution for an $m = 1$ electric quadrupole with $h = 2\pi$, $n_1 = 2.45$ and $n_2 = 1$. The critical angle is 24°. The figure shows the lobe structure in $z > H$ resulting from interference, and it also shows that there is no peak anymore at θ_c.

7. Conclusions

Multipole radiation is shown to possibly have a highly directed peak in its angular intensity distribution when transmitted through an interface. When $r = n_1/n_2 < 1$, there exists an anti-critical angle θ_{ac}, given by $\sin\theta_{ac} = r$, and the possible peak is directed along this angle. We have shown that the possible occurrence of the peak depends on the order (ℓ,m) of the multipole. A magnetic multipole will exhibit this highly directed peak if $\ell + m$ is even, but $m \neq 0$, and an electric multipole has this peak when $\ell + m$ is odd. It is also shown that the peak value is $4/r^3$ times the value of the intensity in the xy-plane for an unbounded multipole. In particular, for $r \lesssim 1$ this factor equals four and $\theta_{ac} \lesssim \pi/2$, indicating that at the slightest deviation from $r = 1$ this peak appears just below the xy-plane, and has a magnitude of four times the value of the intensity in the xy-plane at $r = 1$. For $r \gtrsim 1$, this peak appears just above the xy-plane, but with increasing r the interference between the reflected and directly emitted waves dominates the radiation pattern.

Appendix A

The electromagnetic multipole fields are most conveniently represented in terms of the vector spherical harmonics $\mathbf{T}_{j\ell m}(\theta,\phi)$ [19,20]. The evanescent waves in an angular spectrum representation have wave vectors with an imaginary z-component, which necessitates that we generalize the definition of the vector spherical harmonics [16]. We only need the generalization of $\mathbf{T}_{j\ell m}(\theta,\phi)$ with $j = \ell$. We introduce

$$\mathbf{V}_{\ell m}(\zeta,\phi) = \sum_{\mu}(\ell m - \mu 1\mu|\ell m)S_{\ell,m-\mu}(\zeta,\phi)\mathbf{e}_{\mu}, \tag{A.1}$$

where ζ is complex, ϕ is real, $(\ell m - \mu 1 \mu | \ell m)$ is a Clebsch–Gordan coefficient, the $\mathbf{e}_\mu$ $(\mu = 1,0,-1)$ are the spherical unit vectors, and

$$S_{\ell m}(\zeta, \phi) = \sqrt{\frac{2\ell + 1}{4\pi} \frac{(\ell - m)!}{(\ell + m)!}} P_\ell^m(\zeta) e^{im\phi} \tag{A.2}$$

are generalized spherical harmonics. The functions $P_\ell^m(\zeta)$ are defined as

$$P_\ell^m(\zeta) = (-1)^m (1 - \zeta^2)^{m/2} \frac{d^m}{d\zeta^m} P_\ell(\zeta), m \geqslant 0, \tag{A.3}$$

with $P_\ell(\zeta)$ the Legendre polynomials, and for $m < 0$ we set

$$P_\ell^{-m}(\zeta) = (-1)^m \frac{(\ell - m)!}{(\ell + m)!} P_\ell^m(\zeta). \tag{A.4}$$

In Eq. (A.3) the branch cuts for $(1 - \zeta^2)^{m/2}$ are taken as $(-\infty,-1)$ and $(1,\infty)$. The standard associated Legendre functions are defined by the same formula as Eq. (A.3), but the branch cut is taken as $(-1,1)$. When we set $\zeta = \cos\theta$ in the formulas above, then we have $S_{\ell m}(\cos\theta, \phi) = Y_{\ell m}(\theta, \phi)$ and $\mathbf{V}_{\ell m}(\cos\theta, \phi) = \mathbf{T}_{\ell\ell m}(\theta, \phi)$, which are the regular spherical harmonics and vector spherical harmonics, respectively. The functions $f_{\ell m}(\zeta)$ and $g_{\ell m}(\zeta)$, which determine the intensity distribution of the multipole near an interface, are defined as

$$f_{\ell m}(\zeta) = \frac{1}{|1 - \zeta^2|} |\mathbf{e}_z \cdot \mathbf{V}_{\ell m}(\zeta, 0)|^2, \tag{A.5}$$

$$g_{\ell m}(\zeta) = |\mathbf{e}_y \cdot \mathbf{V}_{\ell m}(\zeta, 0)|^2. \tag{A.6}$$

We now derive some properties of these functions that are used in this paper. The spherical unit vectors $\mathbf{e}_1$ and $\mathbf{e}_{-1}$ are in the xy-plane, so we have from Eq. (A.1)

$$\mathbf{e}_z \cdot \mathbf{V}_{\ell m}(\zeta, \phi) = (\ell m 10 | \ell m) S_{\ell m}(\zeta, \phi), \tag{A.7}$$

with

$$(\ell m 10 | \ell m) = \frac{m}{\sqrt{\ell(\ell + 1)}}. \tag{A.8}$$

Since this Clebsch–Gordan coefficient vanishes for $m = 0$, we have

$$f_{\ell 0}(\zeta) = 0, \tag{A.9}$$

and this gives Eq. (31).

Of particular interest are the values of $f_{\ell m}(\zeta)$ and $g_{\ell m}(\zeta)$ at $\zeta = 0$. The Legendre polynomials are odd and even with ℓ, and with Eqs. (A.3) and (A.4) this gives $P_\ell^m(-\zeta) = (-1)^{\ell+m} P_\ell^m(\zeta)$. Therefore, we have $P_\ell^m(0) = 0$ for $\ell + m$ odd. From Eq. (A.2) we then find

$$S_{\ell m}(0, 0) = 0, \quad \ell + m \text{ odd}. \tag{A.10}$$

By using the explicit expressions for the Legendre polynomials and differentiating m times, it also follows that $P_\ell^m(0) \neq 0$ for $\ell + m$ even, and therefore $S_{\ell m}(0,0) \neq 0$ for $\ell + m$ even. From Eqs. (A.5), (A.7) and (A.8) we then conclude that $f_{\ell m}(0) = 0$ for $\ell + m$ odd and for $m = 0$, and $f_{\ell m}(0) \neq 0$ otherwise.

With $\mathbf{e}_y \cdot \mathbf{e}_\mu = -i/\sqrt{2}$ for $\mu = \pm 1$ we have from Eq. (A.1)

$$\mathbf{e}_y \cdot \mathbf{V}_{\ell m}(\zeta, \phi) = -\frac{i}{\sqrt{2}} \sum_{\mu=\pm 1} (\ell m - \mu 1 \mu | \ell m) S_{\ell, m-\mu}(\zeta, \phi). \tag{A.11}$$

The spherical harmonics satisfy a three-term recursion relation connecting these functions with three different values of m [21], and the same relation holds for the generalized spherical harmonics (with $\cos\theta \to \zeta$). For $\zeta = 0$ the relation reduces to a two-term relation, which can be written as

$$\sum_{\mu=\pm 1} (\ell m - \mu 1 \mu | \ell m) \mu e^{i\mu\phi} S_{\ell, m-\mu}(0, \phi) = 0. \tag{A.12}$$

When we set $\phi = 0$ in Eq. (A.12) and $\zeta = 0$, $\phi = 0$ in Eq. (A.11), then we see that the terms in both summations are the same, except that there is an additional μ in Eq. (A.12). Therefore, for $\zeta = 0$, $\phi = 0$, the two terms in Eq. (A.11) are equal, and we obtain

$$\mathbf{e}_y \cdot \mathbf{V}_{\ell m}(0, 0) = -i\sqrt{2} (\ell m + 1 1 - 1 | \ell m) S_{\ell, m+1}(0, 0). \tag{A.13}$$

Since $S_{\ell, m+1}(0,0) = 0$ for $\ell + m$ even, we find from Eq. (A.6) that $g_{\ell m}(0) = 0$ for $\ell + m$ even. The Clebsch–Gordan coefficient is

$$(\ell m + 1 1 - 1 | \ell m) = \sqrt{\frac{(\ell + m + 1)(\ell - m)}{2\ell(\ell + 1)}}, \tag{A.14}$$

which vanishes only for $m = \ell$. This gives $g_{\ell\ell}(0) = 0$, but this situation is already covered by $g_{\ell m}(0) = 0$ for $\ell + m$ even. From $S_{\ell,m+1}(0,0) \neq 0$ for $\ell + m$ odd (below Eq. (A.10)) we conclude that $g_{\ell m}(0) \neq 0$ for $\ell + m$ odd. In other words, $g_{\ell m}(0)$ does not have an "accidental" zero for $\ell + m$ odd like $f_{\ell m}(0)$ does for $\ell + m$ even.

References

[1] J.D. Jackson, Classical Electrodynamics, third ed., Wiley, New York, 1999 (Section 9.7).
[2] L. Mandel, E. Wolf, Optical Coherence and Quantum Optics, Cambridge University Press, Cambridge, 1995 (Section 3.2).
[3] H.F. Arnoldus, J.T. Foley, J. Opt. Soc. Am. A 19 (2002) 1701.
[4] H.F. Arnoldus, J.T. Foley, Opt. Lett. 28 (2003) 1299.
[5] J. Gasper, G.C. Sherman, J.J. Stamnes, J. Opt. Soc. Am. 66 (1976) 955.
[6] J.E. Sipe, Surf. Sci. 105 (1981) 489.
[7] J.E. Sipe, H.M. van Driel, J.F. Young, Can. J. Phys. 63 (1985) 104.
[8] J.E. Sipe, J. Opt. Soc. B 4 (1987) 481.
[9] M.J.O. Strutt, Ann. d. Phys. Ser. 5 1 (1929) 721.
[10] W. Lukosz, R.E. Kunz, J. Opt. Soc. Am. 67 (1977) 1615.
[11] C.K. Carniglia, L. Mandel, K.H. Drexhage, J. Opt. Soc. Am. 62 (1972) 479.
[12] K.H. Drexhage, Prog. Opt. XII (1974) 163.
[13] A.J. Devaney, E. Wolf, Opt. Commun. 9 (1973) 327.
[14] A.J. Devaney, E. Wolf, J. Math. Phys. 15 (1974) 234.
[15] A. Erdélyi, Physica 4 (1937) 107.
[16] H.F. Arnoldus, Surf. Sci. (submitted).
[17] H.F. Arnoldus, J. Opt. Soc. Am. A 22 (2005) 1.
[18] H.F. Arnoldus, J.T. Foley, J. Opt. Soc. Am. A 21 (2004) 1109.
[19] J.M. Eisenberg, W. Greiner, Excitation Mechanisms of the Nucleus, North-Holland, Amsterdam, 1970 (Chapter 3).
[20] M.E. Rose, Elementary Theory of Angular Momentum, Dover, New York, 1995 (Chapter 7).
[21] E.L. Hill, R. Landshoff, Rev. Mod. Phys. 10 (1938) 87.